Available online at www.sciencedirect.com
SCIENCE DIRECT®
International Journal of Heat and Mass Transfer 48 (2005) 4342–4353
International Journal of HEAT and MASS TRANSFER
www.elsevier.com/locate/ijhmt

A generalized analysis for liquid-fuel vaporization and burning

Randall T. Imaoka, William A. Sirignano *

Department of Mechanical and Aerospace Engineering, University of California Irvine, 3202 Engineering Gateway, Irvine, CA 92697-3975, United States

Received 14 April 2005; received in revised form 21 May 2005
Available online 28 July 2005

Abstract

A generalized method is presented for vaporization and combustion of multiple-droplet arrays, liquid films, pools, and streams. Conditions are explained for the existence of a mass flux potential function that is independent of fuel type and scalar boundary conditions and satisfies the three-dimensional Laplace's equation. Gas-phase properties, composition, and flame location are functions only of the potential function, specified scalar boundary conditions, and fuel type. Variable properties are considered. Flame stand-off distances for liquid interfaces near wet-bulb temperatures are predicted more accurately with variable properties. Flame location and transport properties are found for decane, heptane, and methanol fuels, with different ambient conditions. The analysis also applies to vaporization without combustion and to combustion with transient liquid-phase heating.

Keywords: Liquid-fuel burning; Vaporization; Sprays

1. Introduction

Droplet array vaporization and combustion has been studied extensively with a potential function governing the gas-phase mass flux. Labowsky first utilized the potential function in the absence of Stefan convection [1]. Stefan convection and combustion were considered in subsequent papers [2,3]. The potential function satisfies the three-dimensional Laplace's equation, and accounts for the effects of droplet array size and geometry on vaporization rates. The method has not previously been extended to other configurations for vaporizing or burning liquids. Most of the previous work on droplet array combustion have utilized this transformation to Laplace's equation, and differ mainly in the complexity of the droplet arrays and the method used for solving Laplace's equation. Analytical solutions for two-drop arrays were found by Twardus and Brzustowski [4], Brzustowski et al. [5], and Umemura et al. [6,7]. Sivasankaran et al. [8] studied two droplets with a numerical differencing scheme. Labowsky solved Laplace's equation using a method of images which, in principle, is an exact solution in the form of an infinite series. Marberry et al. [9] and Elperin and Krasovitov [10] both use a method based on the method-of-images but each uniquely modified their method to reduce the error associated with series truncation. A more detailed description of previous work with the advantages and

* Corresponding author. Tel.: +1 949 824 3700; fax: +1 949 824 3773.
E-mail addresses: rimaoka@uci.edu (R.T. Imaoka), sirignan@uci.edu (W.A. Sirignano).

0017-9310/$ - see front matter © 2005 Elsevier Ltd. All rights reserved.
doi:10.1016/j.ijheatmasstransfer.2005.05.018

Nomenclature

a	droplet radius
B	transfer number
c_p	constant pressure specific heat
D	binary diffusion coefficient
h	specific enthalpy
L	latent heat of vaporization
L_{eff}	effective latent heat of vaporization
$\dot{m}$	mass vaporization rate
N	number of species
$\dot{q}$	magnitude of heat flux
Q	heating value per unit mass of fuel
r	radial coordinate
r_{F}	radial flame location
T	temperature
$\vec{V}$	mass-averaged velocity vector
Y	mass fraction

Greek symbols

α	coupling function
η	normalized vaporization rate
λ	thermal conductivity
ν	stoichiometric fuel to oxidizer mass ratio
ρ	mixture density
ϕ	potential function
Φ	normalized potential function
Φ_{F}	flame surface contour
$\dot{\omega}$	rate of mass production per unit volume

Subscripts

F	fuel
iso	isolated droplet
j	the jth droplet
l	liquid
m	the mth species
O	oxidizer
ref	reference value
S	liquid surface value
WB	wet-bulb
∞	ambient value

limitations of various solution methods can be found in [11].

All of the aforementioned work rely on a potential function and the solution to Laplace's equation in their respective geometry. While the modification of vaporization and/or burning rates were presented in each of the cited papers, gas-phase properties and flame contours were seldom given. Since all of the work studying more than two droplets are based on image methods, vaporization or burning rates are readily found without determination of the potential function in the gas-phase. Consequently, flame-surface contours for arrays larger than two droplets are only presented in [11], where a finite-difference scheme was used. Ref. [11] was also the first paper to present individual droplet vaporization rates for more than nine droplets, individual droplet burning rates for more than eight droplets, and individual droplet burning rates in arrays with non-equal interactions for arrays with more than three droplets. Furthermore, in all of the work cited thus far, $\rho D = \lambda/c_p$ was assumed to be constant and transient heating of the liquid was not considered. Quasi-steady vaporization or burning rates were presented in a non-dimensional form normalized by single-droplet values. In this normalized form, the specific calculation of the properties, variable or constant, is not required in the absence of varying liquid temperatures. Dimensional vaporization rates require a specific determination of $\rho D = \lambda/c_p$ whether it is constant or variable. Because the normalized vaporization rates depend only on array size and geometry, the specification of fuel type only becomes necessary in finding the potential contour corresponding to flame location. Even in this case, only properties at the liquid–gas interface are required.

Unlike the previous analyses which focused on specific droplet array geometries, this paper deals with a generalized problem formulation applicable to droplet arrays of any geometry. Theoretical foundations regarding the existence and implications of the potential function has not previously been provided. Several assumptions made in the previous work will be relaxed in the current analysis. Most significantly, a constant value for $\rho D = \lambda/c_p$ will not be required, and this will be shown to have an impact on burning rates and flame locations. Furthermore, the case of vaporization without combustion will not require a unitary Lewis number. The effects of different ambient temperatures and ambient oxidizer mass fractions are presented for decane, heptane, and methanol fuels. Correlations for relevant gas-phase transport properties and flame contour values are given in terms of liquid surface temperatures to aid future liquid-heating calculations. These liquid-heating cases are presented elsewhere [12]. Finally, while not previously demonstrated, the potential function and reduction to Laplace's equation are not restricted to droplet or spray geometries. Liquid–gas interface problems such as liquid films or pools with negligible forced convection can also be treated.

2. Generalized problem formulation

The generalized formulation relies on many of the assumptions used in the cited work. A quasi-steady gas-phase and one-step chemical reaction are required. Fourier heat conduction and Fickian mass diffusion apply. All liquids have identical single-component compositions. Radiation is neglected. Phase equilibrium exists at the liquid surfaces, and the gas is negligibly soluble in the liquid. Kinetic energy, viscous dissipation, and other terms of the order of the square of the Mach number will be neglected. The momentum equation subject to these assumptions yields that the pressure is of the order of the square of the Mach number and, in the calculation of the scalar properties, it can be considered as constant. The steady-state continuity equation, energy conservation, and species conservation equations apply

$$\nabla\cdot(\rho\vec{V})=0, \tag{1}$$

$$\nabla\cdot\left(\rho\vec{V}h-\lambda\nabla T-\sum_{m=1}^{N}\rho D_m h_m\nabla Y_m\right)=-\dot{\omega}_{\mathrm{F}}Q, \tag{2}$$

$$\nabla\cdot\left(\rho\vec{V}Y_m-\rho D_m\nabla Y_m\right)=\dot{\omega}_m\quad m=1,\ldots,N. \tag{3}$$

Sensible mixture enthalpy h, species enthalpy h_m, specific heat c_p, and mixture thermal conductivity λ are computed with the following:

$$h=\int_{T_{\mathrm{ref}}}^{T}c_p(T')\mathrm{d}T',\quad h_m=\int_{T_{\mathrm{ref}}}^{T}c_{p,m}(T')\mathrm{d}T';$$
$$c_p=\sum_m c_{p,m}(T)Y_m;\quad \lambda=\sum_m\lambda_m(T)Y_m. \tag{4}$$

It will be shown in the next section that if there is no tangential velocity at the liquid surface, if scalar properties are uniform on the liquid surface, and if the gas flow is irrotational, the gas-phase mass flux is governed by a potential function ϕ, such that

$$\rho\vec{V}=\nabla\phi. \tag{5}$$

From Eq. (1), ϕ satisfies Laplace's equation and the following boundary conditions:

$$\nabla^2\phi=0\quad\begin{cases}\phi=0 & \text{at liquid surfaces,}\\ \phi=\phi_\infty & \text{far from the liquid.}\end{cases} \tag{6}$$

With a potential function governing mass flux, it then follows that:

$$\nabla\times\rho\vec{V}=\rho(\nabla\times\vec{V})-\vec{V}\times\nabla\rho=0. \tag{7}$$

Therefore, the existence of a potential function requires an irrotational velocity field and the alignment or counter-alignment of the density gradient and velocity vectors throughout the gas-field. As a consequence, velocities at the liquid–gas interface will not have a tangential component since scalar properties are uniform over the liquid surface. Species and energy balances at the liquid surfaces indicate that the quantity $L_{\mathrm{eff}}/(1-Y_{\mathrm{FS}})$ is spatially uniform over all liquid surfaces. Therefore, the instantaneous liquid surface temperature T_{S} and the potential function ϕ will also be spatially uniform at all liquid surfaces. As mentioned, verification of the existence of a potential function will be given in Section 2.1. The equations shown here will apply to vaporization with and without combustion. Simplifications and additional assumptions will be made as needed.

2.1. Analysis of vaporization without combustion

In the absence of combustion, no additional assumptions are necessary. Eqs. (2) and (3) are reduced to

$$\nabla\cdot(\rho\vec{V}h-\lambda\nabla T-\sum_{m=1}^{N}\rho D_m h_m\nabla Y_m)=0, \tag{8}$$

$$\nabla\cdot\left(\rho\vec{V}Y_m-\rho D_m\nabla Y_m\right)=0\quad m=1,\ldots,N. \tag{9}$$

From Eqs. (1) and (9), it follows that:

$$\nabla\cdot(\rho\vec{V}Y_m-\rho D_m\nabla Y_m-C_m\rho\vec{V})=0,\quad m=1,\ldots,N, \tag{10}$$

where C_m is a constant. Assume Y_m is uniform over the liquid surface and $\vec{V}$ is normal to the liquid surface. Choose C_m so that

$$(\rho\vec{V}Y_m)_{\mathrm{S}}-(\rho D_m\nabla Y_m)_{\mathrm{S}}-(C_m\rho\vec{V})_{\mathrm{S}}=0\quad m=1,\ldots,N \tag{11}$$

is satisfied at the liquid boundary. Then, define

$$\rho\vec{V}Y_m-\rho D_m\nabla Y_m-C_m\rho\vec{V}=\vec{\Psi}_m\quad m=1,\ldots,N, \tag{12}$$

where $\vec{\Psi}_m=0$ at the liquid surface from (11), and from (12), $\nabla\cdot\vec{\Psi}_m=0$ throughout the gas-field. Note further that $\rho\vec{V}$ and ∇Y_m go to zero at infinity; so $\vec{\Psi}_m=0$ there. The only solution is $\vec{\Psi}_m=0$. Therefore

$$(Y_m-C_m)\rho\vec{V}-\rho D_m\nabla Y_m=0\quad m=1,\ldots,N \tag{13}$$

throughout the field. Applying the same analysis to the energy equation with a uniform temperature over the liquid surface, and noting that ∇h goes to zero at infinity

$$(h-C)\rho\vec{V}-\lambda\nabla T-\sum_{m=1}^{N}\rho D_m h_m\nabla Y_m=0. \tag{14}$$

Consequently, the heat and mass diffusion flux vectors are aligned (or counter-aligned) with the streamlines. The same analysis can be applied in the next subsection to the equation governing the scalar coupling functions. Since the mass fractions and enthalpy have gradients aligned with the velocity vector, and the pressure variation is insignificant, the density gradient will be locally parallel to the streamlines. Note that for a quasi-steady inviscid flow, the fractional pressure variations are of the order of the square of the Mach number. As shown

by Joseph [13,14], constant density flows with normal viscous stress can be irrotational. In that case, fractional variations in the thermodynamic pressure can be of the order of the Mach number. So, viscosity could be considered in our potential flow analysis if the constant-density assumption were invoked. With an irrotational flow, Eq. (7) is satisfied and the mass-flux potential may be used.

$$(Y_m - C_m)\nabla\phi - \rho D_m \nabla Y_m = 0 \quad m = 1, \ldots, N, \tag{15}$$

$$(h - C)\nabla\phi - \lambda\nabla T - \sum_{m=1}^{N} \rho D_m h_m \nabla Y_m = 0. \tag{16}$$

Species mass balance at the liquid–gas interface indicates that $C_m = 0$ for $m \neq F$, and $C_F = 1$. Eq. (15) is multiplied by h_m and summed for all species. The result is subtracted from (16). Energy balance at the interface yields the constant C, and noting that $\nabla T = (\nabla h_F)/c_{p,F}$

$$\nabla \ln(h_F - h_{FS} + L_{eff}) = \frac{\nabla\phi}{\lambda/c_{p,F}}, \tag{17}$$

$$L_{eff} = L + \frac{\dot{q}_l}{|\rho\vec{V}|_S}. \tag{18}$$

The term $\dot{q}_l$ is the magnitude of the conductive heat flux into the liquid when droplets are not at wet-bulb temperatures. With the arbitrariness of a constant in the determination of ϕ, taking $\phi_S = 0$ incurs no loss of generality. The implicit relation between h_F and ϕ is obtained by integrating Eq. (17) along a pathline to yield

$$1 + \frac{h_F - h_{FS}}{L_{eff}} = (1 + B_H)e^{-\int_{\phi}^{\phi_\infty} \frac{d\phi'}{\lambda/c_{p,F}}}, \tag{19}$$

where

$$B_H = \frac{h_{F\infty} - h_{FS}}{L_{eff}}. \tag{20}$$

Evaluation of Eq. (19) at infinity, we obtain

$$\phi_\infty = \overline{\lambda/c_{p,F}} \ln(1 + B_H), \tag{21}$$

where the definition is made that

$$\overline{\lambda/c_{p,F}} = \frac{\phi_\infty}{\int_0^{\phi_\infty} \frac{d\phi'}{\lambda/c_{p,F}}}. \tag{22}$$

A normalized potential function Φ is defined such that

$$\Phi = \frac{\phi}{\phi_\infty}. \tag{23}$$

Eqs. (19) and (22) can now be written as functions of Φ

$$1 + \frac{h_F - h_{FS}}{L_{eff}} = (1 + B_H)^{\overline{\lambda/c_{p,F}} \int_0^{\Phi} \frac{d\Phi'}{\lambda/c_{p,F}}}, \tag{24}$$

$$\overline{\lambda/c_{p,F}} = \left(\int_0^1 \frac{d\Phi'}{\lambda/c_{p,F}} \right)^{-1}. \tag{25}$$

From Eqs. (1), (6), and (23), the normalized potential function in any geometry satisfies Laplace's equation with the following boundary conditions:

$$\nabla^2\Phi = 0 \quad \begin{cases} \Phi = 0 & \text{at liquid surfaces,} \\ \Phi = 1 & \text{far from the liquid.} \end{cases} \tag{26}$$

The species equations are treated in a process similar to the energy equation. Integration of (15) for each of the N species, and using the relations given in Eqs. (21) and (23), we obtain

$$\frac{Y_F - 1}{Y_{FS} - 1} = (1 + B_H)^{\overline{\lambda/c_{p,F}} \int_0^{\Phi} \frac{d\Phi'}{\rho D_F}} \quad m = F, \tag{27}$$

$$\frac{Y_m}{Y_{m\infty}} = (1 + B_H)^{\overline{\lambda/c_{p,F}} \int_0^{\Phi} \frac{d\Phi'}{\rho D_m} Le_m} \quad m \neq F. \tag{28}$$

The following relations are defined:

$$Le_m = \frac{\overline{\lambda/c_{p,F}}}{\overline{\rho D_m}} \tag{29}$$

$$\overline{\rho D_m} = \left(\int_0^1 \frac{d\Phi'}{\rho D_m} \right)^{-1} \tag{30}$$

$$B_M = \frac{Y_{FS} - Y_{F\infty}}{1 - Y_{FS}} \tag{31}$$

The relationship between B_M and B_H is given by

$$1 + B_M = (1 + B_H)^{Le_F}. \tag{32}$$

Solutions to Eqs. (24), (27), and (28) yield the relationship between the gas-field properties and the normalized potential function Φ with a variable Lewis number and variable ρD, where Φ is governed by Eq. (26).

2.2. Combustion analysis

The formulation presented earlier in Section 2 applies here with several additional assumptions. Fast chemical kinetics prevents oxygen from diffusing to the liquid surface, and a unitary Lewis number, $\rho D = \lambda/c_p$, is required. The Shvab–Zeldovich form of the species and energy conservation equations apply

$$\nabla \cdot (\rho\vec{V}\alpha_i - \rho D \nabla\alpha_i) = 0, \quad i = 1, 2. \tag{33}$$

The coupling functions are defined as

$$\alpha_1 = h + \nu Q Y_O, \quad \alpha_2 = Y_F - \nu Y_O. \tag{34}$$

Consistent with the analysis of the previous sections, the advection and diffusion of the scalar variables (34) are aligned with the flow

$$\rho\vec{V}\alpha_i - \rho D\nabla\alpha_i = A_i\rho\vec{V}, \quad i = 1, 2. \tag{35}$$

Substitution of (5) into (35) and rearranging, it then follows that:

$$\nabla \ln(\alpha_i - A_i) = \frac{\nabla\phi}{\rho D}. \quad i = 1, 2. \tag{36}$$

Integrating along any path, and setting $\phi = 0$ at the liquid surfaces

$$\frac{\alpha_i - A_i}{\alpha_{i,\mathrm{S}} - A_i} = \mathrm{e}^{\int_0^{\phi} \frac{\mathrm{d}\phi'}{\rho D}}, \quad i = 1, 2. \tag{37}$$

Note that this solution for the coupling function α_i is consistent with the literature when $\rho D = \text{constant}$. Evaluation of Eq. (37) in the far-field yields the relation for ϕ_∞

$$\phi_\infty = \overline{\rho D} \ln\left(\frac{\alpha_{i,\infty} - A_i}{\alpha_{i,\mathrm{S}} - A_i}\right) = \overline{\rho D} \ln(1 + B) \quad i = 1, 2. \tag{38}$$

The definitions are made that

$$\overline{\rho D} = \frac{\phi_\infty}{\int_0^{\phi_\infty} \frac{\mathrm{d}\phi'}{\rho D}}, \tag{39}$$

$$B = \frac{h_\infty - h_\mathrm{S} + vQY_{\mathrm{O}\infty}}{L_{\mathrm{eff}}} = \frac{vY_{\mathrm{O}\infty} + Y_{\mathrm{FS}}}{1 - Y_{\mathrm{FS}}}, \tag{40}$$

where L_{eff} is given by Eq. (18). Since $Le = 1$ implies that $\rho D = \lambda/c_p$, these values will be used interchangeably wherever necessary. Eqs. (23), (37) and (38) are combined to yield

$$\frac{\alpha_i - A_i}{\alpha_{i,\mathrm{S}} - A_i} = (1 + B)^{\frac{\overline{\rho D}}{\int_0^{\Phi} \frac{\mathrm{d}\Phi'}{\lambda/c_p}}}. \tag{41}$$

Application of boundary conditions provides the values of A_i. Then, from Eqs. (34) and (41)

$$(1 + B)^{\frac{\overline{\rho D}}{\int_0^{\Phi} \frac{\mathrm{d}\Phi'}{\lambda/c_p}}} = 1 + \frac{h - h_\mathrm{S} + vQY_\mathrm{O}}{L_{\mathrm{eff}}} = 1 + \frac{Y_\mathrm{F} - Y_{\mathrm{FS}} - vY_\mathrm{O}}{Y_{\mathrm{FS}} - 1}. \tag{42}$$

Noting that $Le = 1$, the combination of Eqs. (23), (38), and (39) yields the following relation:

$$\overline{\rho D} = \overline{\lambda/c_p} = \left(\int_0^1 \frac{\mathrm{d}\Phi'}{\lambda/c_p}\right)^{-1}. \tag{43}$$

In the limit of infinite-rate chemical kinetics, the flame surface will lie on the constant Φ surface denoted by Φ_F. This value is determined implicitly via the following expression:

$$\frac{\ln(1 - Y_{\mathrm{FS}})}{\ln(1 + B)} = -\overline{\rho D} \int_0^{\Phi_\mathrm{F}} \frac{\mathrm{d}\Phi'}{\lambda/c_p}. \tag{44}$$

The system of Eqs. (42)–(44) yield the four relations necessary to determine the values of $\overline{\rho D}$, the flame contour Φ_F, mixture enthalpy h, and fuel vapor mass fraction Y_F. Fuel type, T_∞, $Y_{\mathrm{O}\infty}$, and T_S are treated as parameters in the calculations. Eqs. (42) and (43) are coupled because transport properties and specific heat depend on temperature and composition. When the liquid surface temperature is less than the wet-bulb value, phase equilibrium dictates that B be calculated with the last term in Eq. (40). The first term then provides the liquid heating rate through L_{eff}. Note that ρD was not assumed constant in the analysis. With the assumption $\rho D = \lambda/c_p = \overline{\rho D} = \text{constant}$, Eqs. (42)–(44) are simplified and uncoupled. Then

$$(1 + B)^{\Phi} = 1 + \frac{h - h_\mathrm{S} + vQY_\mathrm{O}}{L_{\mathrm{eff}}} = 1 + \frac{Y_\mathrm{F} - Y_{\mathrm{FS}} - vY_\mathrm{O}}{Y_{\mathrm{FS}} - 1}, \tag{45}$$

$$\Phi_\mathrm{F} = \frac{-\ln(1 - Y_{\mathrm{FS}})}{\ln(1 + B)}. \tag{46}$$

Eqs. (45) and (46) would still result if the constant value of $\rho D = \lambda/c_p$ were defined arbitrarily, without accordance to Eq. (43). For example, if the value is taken at infinity or at the liquid surface.

In either the variable ρD or constant ρD situation, the vaporization rate of the jth droplet (or any portion of the liquid surface designated as the jth segment) is obtained by integrating the mass flux over the droplet (segment) surface

$$\dot{m}_j = \int\int \nabla\phi \cdot \mathrm{d}\vec{A}_j = \overline{\rho D} \ln(1 + B) \int\int \nabla\Phi \cdot \mathrm{d}\vec{A}_j \tag{47}$$

It is not uncommon for droplet vaporization rates to be normalized by the vaporization rate of an isolated droplet at the wet-bulb temperature. In the literature, this has often been referred to as a burning rate correction factor or an interaction coefficient, η. Then, for the jth droplet

$$\eta_j = \frac{\dot{m}_j}{\dot{m}_{\mathrm{iso}}} = \frac{1}{4\pi a_j} \int\int \nabla\Phi \cdot \mathrm{d}\vec{A}_j. \tag{48}$$

The vaporization rate of an isolated droplet at wet-bulb temperature with variable $\rho D = \lambda/c_p$ is given by

$$\dot{m}_{\mathrm{iso}} = 4\pi \left(\int_a^\infty \frac{\mathrm{d}r}{(\lambda/c_p) r^2}\right)^{-1} \ln(1 + B). \tag{49}$$

For a single, isolated droplet, the solution to Eq. (26) yields $\Phi_{\mathrm{iso}} = 1 - a/r$. Upon substitution with (43), Eq. (49) can be expressed as

$$\dot{m}_{\mathrm{iso}} = 4\pi a \overline{\rho D} \ln(1 + B). \tag{50}$$

Therefore, within this generalized analysis, a single, isolated droplet is a special case for which the solution Φ to Eq. (26) can be obtained analytically.

The use of normalized vaporization rates as in Eq. (48) has been the standard for authors studying multiple droplet arrays. Although this practice does provide an assessment of the effect of droplet interactions, several key aspects are obscured. To obtain an actual (dimensional) vaporization rate, one would refer to Eq. (48) with η known for a specific geometry. However, the vaporization rate of an isolated droplet, and more specifically the value of $\rho D = \lambda/c_p$, is not obvious. In all of the cited work ρD is assumed constant, yet in practice it will vary spatially in the gas-phase. No

mention of the appropriate value, or an appropriate average value has ever been presented. This is possibly due to the absence of liquid-heating, where the numerical value of $\rho D = \lambda/c_p$ would have been required. Law [15], and Law and Sirignano [16] include liquid-phase heating for an isolated drop but use a constant value for ρD. Another shortcoming of a normalized vaporization rate involves its applicability to array geometry optimization. For example, would a larger number of smaller droplets result in higher burning rates? This issue, along with a transient liquid-phase heating analysis are discussed in [12].

The analysis applies universally to all droplet array sizes and geometries. As previously mentioned, other liquid–gas interface problems are also included. Geometrical effects are calculated separately through the potential function Φ, and are independent of gas-phase transport properties and boundary conditions. Consequently, the problem for the scalar properties is one-dimensional for any configuration while the three-dimensional analysis is necessary only in solving Eq. (26). Although no solutions to Laplace's equation will be presented here, quasi-steady results for droplet arrays of various configurations can be found in the references. The coupled Eqs. (42)–(44) are solved numerically with variable properties computed with Eq. (4). The iterative solution takes $\rho D = \lambda/c_p = \overline{\rho D}$ as a first approximation. Mixture composition and enthalpy are then determined as a function of Φ from Eq. (42), and used in (43) and (44) to determine $\overline{\rho D}$ and Φ_F. The same mixture composition is used in (42), but with the newly computed $\overline{\rho D}$ and Φ_F to yield updated mixture compositions and enthalpies. The process is repeated, with good convergence after approximately 20 iterations.

3. Results and discussion

The scalar quantities T, Y_F, and Y_O are shown versus Φ in Fig. 1a–c for decane, heptane, and methanol fuels, with $T_\infty = 298$ K and $Y_{O\infty} = 0.231$. The ambient pressure is one atmosphere in all of the calculations. The large variation in flame location for decane indicated by Fig. 1a is caused by the larger wet-bulb temperature and lower volatility resulting in lower values of Y_{FS} at 298 K than for the other fuels. Mixture temperatures and composition are shown in Fig. 2 for decane with similar boundary conditions as in Fig. 1a, except with $Y_{O\infty} = 0.75$. As shown in Fig. 2, an increase in ambient oxidizer mass fraction leads to higher flame temperatures and brings the flame closer to the liquid surface as expected. The proximity of the flame to the liquid surface for a low volatility fuel introduces the possibility of individual droplet flames for low droplet surface temperatures. However, the occurrence of individual flames will depend strongly on the array geometry.

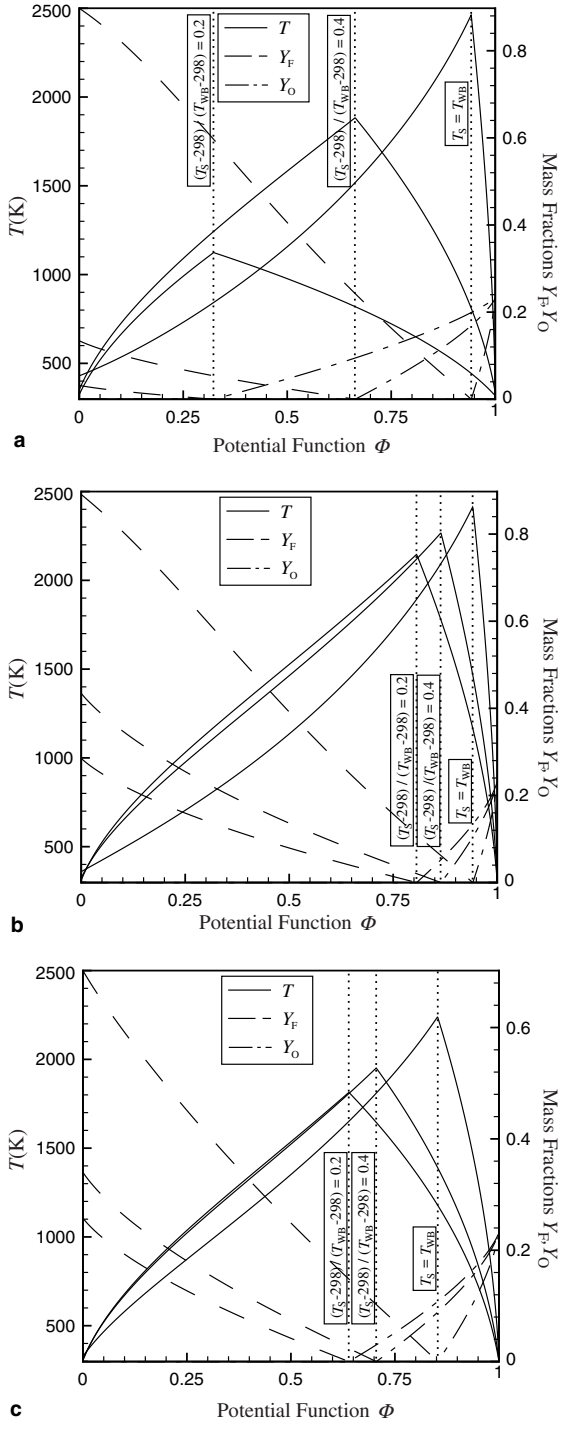

Fig. 1. Temperature, fuel and oxidizer mass fractions versus Φ with $T_\infty = 298$ and $Y_{O\infty} = 0.231$ for various surface temperatures: (a) decane, $T_{WB} = 429.73$ K; (b) heptane, $T_{WB} = 359.36$ K and (c) methanol, $T_{WB} = 327.44$ K.

Fig. 3 shows $\overline{\rho D}$ and Φ_F versus liquid surface temperature for decane with different oxidizer mass fractions.

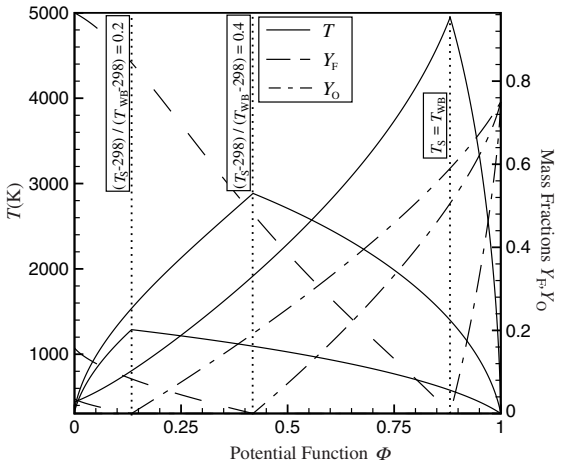

Fig. 2. Temperature, fuel and oxidizer mass fractions for decane with $T_\infty = 298$ K and $Y_{O\infty} = 0.75$ for various surface temperatures. $T_{WB} = 440.62$ K.

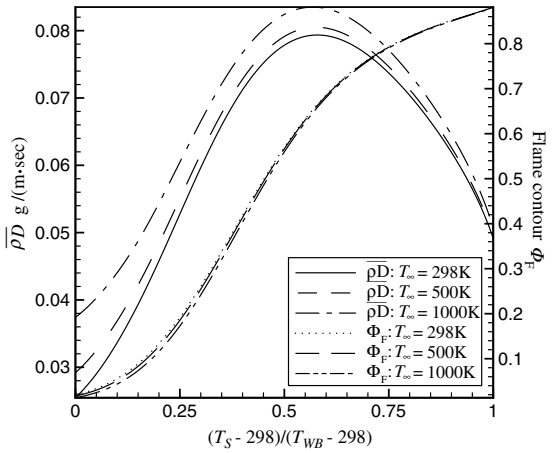

Fig. 4. The effect of T_∞ on $\overline{\rho D}$ and Φ_F is shown versus surface temperature for decane with $Y_{O\infty} = 0.75$. Wet-bulb temperatures are 440.62 K, 440.74 K, and 441.06 K for $T_\infty = 298$ K, 500 K, and 1000 K, respectively.

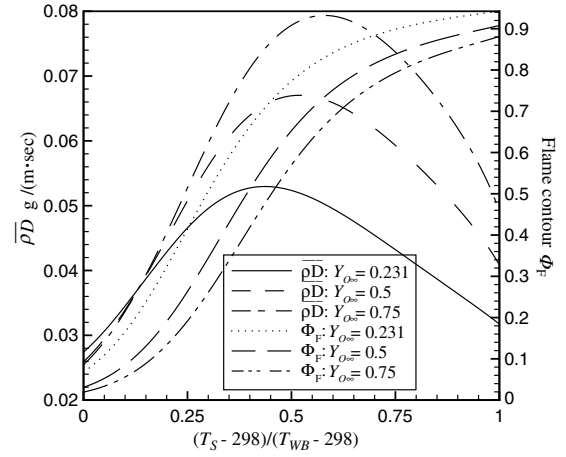

Fig. 3. The effect of $Y_{O\infty}$ on $\overline{\rho D}$ and Φ_F is shown versus surface temperature for decane with $T_\infty = 298$ K. Wet-bulb temperatures are 429.73 K, 437.96 K, and 440.62 K for $Y_{O\infty} = 0.231$, 0.5, and 0.75, respectively.

The effect of ambient temperature on $\overline{\rho D}$ and Φ_F is illustrated in Fig. 4 for decane with $Y_{O\infty} = 0.75$. Comparisons of $\overline{\rho D}$ and Φ_F for decane, heptane, and methanol are shown in Fig. 5a for $Y_{O\infty} = 0.231$, and Fig. 5b for $Y_{O\infty} = 0.75$. The monotonic increase in Φ_F with liquid surface temperature is expected. The behavior of $\overline{\rho D}$ is noteworthy. For decane, $\overline{\rho D}$ exhibits a local maximum that is more pronounced than with heptane or methanol. This occurs with decane because of the large variation in flame location due to surface temperature. Note that λ/c_p depends on mixture temperature, and also that flame temperatures (and therefore λ/c_p) and flame standoff distances (in terms of Φ) increase with liquid surface temperature. Therefore, the integral in Eq. (43) is minimized when the flame is located at some intermediate distance from the droplet surface. In Figs. 3–5b, the effect of increasing $Y_{O\infty}$ is to increase the magnitude of $\overline{\rho D}$ (due to higher mixture temperatures) and shift the local maximum to higher Φ values (since flames will exist closer to the liquid surface with increasing $Y_{O\infty}$). With heptane and methanol, Φ_F will not vary over as broad a range as with decane, hence the local maxima are less obvious.

$\overline{\rho D}$ and Φ_F depend upon fuel type and scalar boundary conditions. Therefore, to facilitate future calculations, correlations for $\overline{\rho D}$ and Φ_F with surface temperature are given in Tables 1–6 for decane, heptane, and methanol with different boundary conditions. As permitted by the unitary Lewis number, λ/c_p has been used in Eqs. (42)–(44). Note that the data presented in Tables 1–6 are applicable only with the specified boundary conditions. From Fig. 4, ambient temperature is shown to have a moderate effect on $\overline{\rho D}$, but a negligible effect on the determination of Φ_F. However, changes in $Y_{O\infty}$ will strongly affect both $\overline{\rho D}$ and Φ_F. Eqs. (42)–(44) need to be solved with the appropriate fuel type and boundary conditions.

With the assumption $\rho D = $ constant, the coupled system of integral Eqs. (42)–(44) are reduced to (45) and (46), which are independent of ρD. However, since $\overline{\rho D}$ is necessary to calculate actual vaporization rates or for liquid-heating calculations, using Eq. (43) together with (45) and (46) will provide the mathematically correct weighted average of ρD to be used with the constant ρD assumption. The value of $\overline{\rho D}$ computed in this manner is considered to be based on the constant ρD assumption, and is preferable to using a value at the

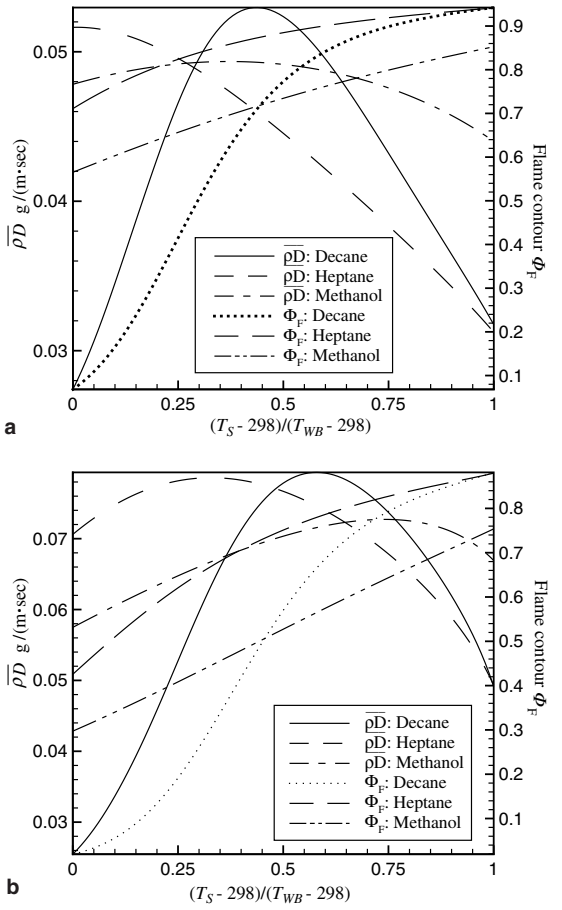

Fig. 5. $\overline{\rho D}$ and Φ_F are shown versus surface temperature for decane, heptane, and methanol with $T_\infty = 298$ K: (a) $Y_{O\infty} = 0.231$, wet-bulb temperatures are 429.73 K, 359.36 K, and 327.44 K for decane, heptane, and methanol, respectively and (b) $Y_{O\infty} = 0.75$, wet-bulb temperatures are 440.62 K, 366.93 K, and 332.97 K for decane, heptane, and methanol, respectively.

liquid surface, far-field, or other arbitrarily chosen average. This will be termed as an "average" ρD. The first iteration of the solution to Eqs. (42)–(44) with $\rho D = \lambda/c_p = \overline{\rho D}$ will yield this average value.

Note that Eq. (43) is not a volume-weighted average of λ/c_p in the gas-phase. The integral in Φ will emphasize (spatially) the volume near the liquid where the magnitude of $\nabla\Phi$ is large, and will tend to give less emphasis to the far-field despite the considerable volume located far from the droplets. A comparison between $\overline{\rho D}$ based on the averaged value and $\overline{\rho D}$ obtained through solution of Eqs. (42)–(44) is shown in Fig. 6 for decane, heptane, and methanol with $T_\infty = 298$ K and $Y_{O\infty} = 0.231$. The constant ρD assumption does not significantly alter $\overline{\rho D}$ near wet-bulb temperatures. Fortunately, all of the literature on quasi-steady droplet array vaporization or combustion deal with droplets at wet-bulb temperatures. The discrepancy at lower liquid surface temperatures is more pronounced and will impact liquid heating rates in transient calculations. At 298 K, $\overline{\rho D}$ based on the average value exceeds the exact value by more than 40% for decane yet underestimates the exact value by 1.3% for heptane.

Flame surface contour values Φ_F will also vary when computed with Eq. (44) versus Eq. (46). This is illustrated in Fig. 7 for the three fuels with $T_\infty = 298$ K and $Y_{O\infty} = 0.231$. Values for Φ_F obtained with Eq. (46) are consistently larger, indicating greater flame stand-off distances. While the percent difference between Φ_F values obtained with and without the constant ρD assumption do not change significantly with liquid surface temperature, the translation to actual stand-off distance is more dramatic. With $\nabla\Phi \to 0$ for large distances, actual flame locations become strongly dependent on Φ_F as $\Phi_F \to 1$ in the far-field. Flame stand-off distances for isolated droplets are shown in Fig. 8 using Φ_F values from Eqs. (44) and (46). The extent to which Eq. (46) overestimates flame stand-off distances at wet-bulb temperatures is substantial. The use of an average ρD over-predicts flame stand-off distances by factors of 2.11, 2.09, and 1.39 for decane, heptane, and methanol at their respective wet-bulb temperatures. These factors will increase slightly to 2.15, 2.13, and 1.42 when

Table 1
Curve-fit coefficients for $\overline{\rho D} = \overline{\lambda/c_p}$ (g/m s) and Φ_F as a function of surface temperature with $T_\infty = 298$ K and $Y_{O\infty} = 0.231$

	Decane: $T_{WB} = 429.73$ K		Heptane: $T_{WB} = 359.36$ K		Methanol: $T_{WB} = 327.44$ K	
	$\overline{\rho D} = \overline{\lambda/c_p}$	Φ_F	$\overline{\rho D} = \overline{\lambda/c_p}$	Φ_F	$\overline{\rho D} = \overline{\lambda/c_p}$	Φ_F
a_0	1.1409991E+02	−6.9280734E+02	1.7972100E+01	−2.1186766E+02	4.5582964E+02	9.5487600E+02
a_1	−1.6938311E+00	1.5254532E+01	−3.2627383E−01	2.7093006E+00	−7.4235815E+00	−1.4408079E+01
a_2	1.0276693E−02	−1.3010970E−01	2.2927641E−03	−1.3791967E−02	4.8334587E−02	8.5992197E−02
a_3	−3.2540528E−05	5.6362410E−04	−7.8475187E−06	3.5053468E−05	−1.5729774E−04	−2.5375005E−04
a_4	5.6537302E−08	−1.3253211E−06	1.3167346E−08	−4.4438132E−08	2.5593365E−07	3.7025159E−07
a_5	−5.0835936E−11	1.6175097E−09	−8.7076543E−12	2.2464770E−11	−1.6660221E−10	−2.1355782E−10
a_6	1.8311169E−14	−8.0507140E−13				

$\overline{\rho D}, \Phi_F = a_0 + a_1 T_S + a_2 T_S^2 + a_3 T_S^3 + a_4 T_S^4 + a_5 T_S^5 + a_6 T_S^6$ (298 K $\leqslant T_S$(K) $\leqslant T_{WB}$).

Table 2
Curve-fit coefficients for $\overline{\rho D} = \overline{\lambda/c_p}$ (g/m s) and Φ_F as a function of surface temperature with $T_\infty = 298$ K and $Y_{O\infty} = 0.5$

	Decane: $T_{WB} = 437.96$ K		Heptane: $T_{WB} = 365.09$ K		Methanol: $T_{WB} = 331.62$ K	
	$\overline{\rho D} = \overline{\lambda/c_p}$	Φ_F	$\overline{\rho D} = \overline{\lambda/c_p}$	Φ_F	$\overline{\rho D} = \overline{\lambda/c_p}$	Φ_F
a_0	−6.6162770E+01	−3.8947800E+03	1.2216370E+02	4.4219475E+02	1.5519001E+03	−2.8653131E+03
a_1	1.3282320E+00	6.5867670E+01	−1.9237116E+00	−6.9357188E+00	−2.5067550E+01	4.7501479E+01
a_2	−1.0680260E−02	−4.6067990E−01	1.2060450E−02	4.2852367E−02	1.6196203E−01	−3.1436608E−01
a_3	4.4410670E−05	1.7055630E−03	−3.7636245E−05	−1.3069499E−04	−5.2325717E−04	1.0377826E−03
a_4	−1.0129130E−07	−3.5259770E−06	5.8505657E−08	1.9733933E−07	8.4540568E−07	−1.7084663E−06
a_5	1.2067060E−10	3.8607590E−09	−3.6273151E−11	−1.1823890E−10	−5.4650435E−10	1.1220888E−09
a_6	−5.8867090E−14	−1.7499690E−12				

$\overline{\rho D}, \Phi_F = a_0 + a_1 T_S + a_2 T_S^2 + a_3 T_S^3 + a_4 T_S^4 + a_5 T_S^5 + a_6 T_S^6$ (298 K $\leqslant T_S$ (K) $\leqslant T_{WB}$).

Table 3
Curve-fit coefficients for $\overline{\rho D} = \overline{\lambda/c_p}$ (g/m s) and Φ_F as a function of surface temperature with $T_\infty = 298$ K and $Y_{O\infty} = 0.75$

	Decane: $T_{WB} = 440.62$ K		Heptane: $T_{WB} = 366.93$ K		Methanol: $T_{WB} = 332.97$ K	
	$\overline{\rho D} = \overline{\lambda/c_p}$	Φ_F	$\overline{\rho D} = \overline{\lambda/c_p}$	Φ_F	$\overline{\rho D} = \overline{\lambda/c_p}$	Φ_F
a_0	−2.2195020E+02	−4.0495110E+03	2.4234938E+02	8.3738030E+02	2.8022377E+03	−6.0042483E+03
a_1	3.8761490E+00	6.6938360E+01	−3.7485112E+00	−1.2556305E+01	−4.5142295E+01	9.7188321E+01
a_2	−2.7930220E−02	−4.5781820E−01	2.3122079E−02	7.4679529E−02	2.9088726E−01	−6.2845708E−01
a_3	1.0629800E−04	1.6582910E−03	−7.1114268E−05	−2.2044105E−04	−9.3726464E−04	2.0290175E−03
a_4	−2.2541950E−07	−3.3556380E−06	1.0911728E−07	3.2339673E−07	1.5101650E−06	−3.2704166E−06
a_5	2.5269590E−10	3.5980320E−09	−6.6862496E−11	−1.8880698E−10	−9.7347081E−10	2.1053956E−09
a_6	−1.1707460E−13	−1.5977240E−12				

$\overline{\rho D}, \Phi_F = a_0 + a_1 T_S + a_2 T_S^2 + a_3 T_S^3 + a_4 T_S^4 + a_5 T_S^5 + a_6 T_S^6$ (298 K $\leqslant T_S$ (K) $\leqslant T_{WB}$).

Table 4
Curve-fit coefficients for $\overline{\rho D} = \overline{\lambda/c_p}$ (g/m s) and Φ_F as a function of surface temperature with $T_\infty = 1000$ K and $Y_{O\infty} = 0.231$

	Decane: $T_{WB} = 432.80$ K		Heptane: $T_{WB} = 361.51$ K		Methanol: $T_{WB} = 329.14$ K	
	$\overline{\rho D} = \overline{\lambda/c_p}$	Φ_F	$\overline{\rho D} = \overline{\lambda/c_p}$	Φ_F	$\overline{\rho D} = \overline{\lambda/c_p}$	Φ_F
a_0	6.7217369E+01	−3.7624394E+02	2.8856566E+01	−2.2672283E+02	6.0736739E+02	6.8729452E+02
a_1	−9.2629444E−01	9.9507754E+00	−4.9150489E−01	2.9270726E+00	−9.8603853E+00	−9.9879420E+00
a_2	5.0622875E−03	−9.3054160E−02	3.2965380E−03	−1.5083249E−02	6.4010604E−02	5.6822662E−02
a_3	−1.3716876E−05	4.2546193E−04	−1.0896942E−05	3.8917925E−05	−2.0772403E−04	−1.5764001E−04
a_4	1.8445469E−08	−1.0354751E−06	1.7799610E−08	−5.0266349E−08	3.3704359E−07	2.1215631E−07
a_5	−9.8580378E−12	1.2932523E−09	−1.1522436E−11	2.6003527E−11	−2.1879011E−10	−1.0969423E−10
a_6		−6.5400539E−13				

$\overline{\rho D}, \Phi_F = a_0 + a_1 T_S + a_2 T_S^2 + a_3 T_S^3 + a_4 T_S^4 + a_5 T_S^5 + a_6 T_S^6$ (298 K $\leqslant T_S$ (K) $\leqslant T_{WB}$).

Table 5
Curve-fit coefficients for $\overline{\rho D} = \overline{\lambda/c_p}$ (g/m s) and Φ_F as a function of surface temperature with $T_\infty = 1000$ K and $Y_{O\infty} = 0.5$

	Decane: $T_{WB} = 438.85$ K		Heptane: $T_{WB} = 365.71$ K		Methanol: $T_{WB} = 332.16$ K	
	$\overline{\rho D} = \overline{\lambda/c_p}$	Φ_F	$\overline{\rho D} = \overline{\lambda/c_p}$	Φ_F	$\overline{\rho D} = \overline{\lambda/c_p}$	Φ_F
a_0	−7.7140812E+01	−4.1622188E+03	1.4220318E+02	4.6752118E+02	1.8237532E+03	−3.4848327E+03
a_1	1.4915501E+00	7.0228395E+01	−2.2248455E+00	−7.3119532E+00	−2.9431074E+01	5.7468166E+01
a_2	−1.1674318E−02	−4.9006906E−01	1.3872196E−02	4.5062196E−02	1.8998059E−01	−3.7842926E−01
a_3	4.7579683E−05	1.8103781E−03	−4.3090036E−05	−1.3712154E−04	−6.1321656E−04	1.2434220E−03
a_4	−1.0686595E−07	−3.7346827E−06	6.6719339E−08	2.0660373E−07	9.8982510E−07	−2.0381041E−06
a_5	1.2578962E−10	4.0808233E−09	−4.1224351E−11	−1.2353895E−10	−6.3924350E−10	1.3331937E−09
a_6	−6.0777006E−14	−1.8459995E−12				

$\overline{\rho D}, \Phi_F = a_0 + a_1 T_S + a_2 T_S^2 + a_3 T_S^3 + a_4 T_S^4 + a_5 T_S^5 + a_6 T_S^6$ (298 K $\leqslant T_S$ (K) $\leqslant T_{WB}$).

Table 6
Curve-fit coefficients for $\overline{\rho D} = \overline{\lambda/c_p}$ (g/m s) and Φ_F as a function of surface temperature with $T_\infty = 1000$ K and $Y_{O\infty} = 0.75$

	Decane: $T_{WB} = 441.06$ K		Heptane: $T_{WB} = 367.24$ K		Methanol: $T_{WB} = 333.26$ K	
	$\overline{\rho D} = \overline{\lambda/c_p}$	Φ_F	$\overline{\rho D} = \overline{\lambda/c_p}$	Φ_F	$\overline{\rho D} = \overline{\lambda/c_p}$	Φ_F
a_0	−2.2299130E+02	−4.4354502E+03	2.6606771E+02	9.1448930E+02	3.1823094E+03	−6.6134922E+03
a_1	3.8742307E+00	7.3165929E+01	−4.1039982E+00	−1.3694516E+01	−5.1240790E+01	1.0692724E+02
a_2	−2.7786377E−02	−4.9941044E−01	2.5257252E−02	8.1367671E−02	3.3003071E−01	−6.9063176E−01
a_3	1.0531741E−04	1.8054976E−03	−7.7536456E−05	−2.4001274E−04	−1.0628851E−03	2.2271671E−03
a_4	−2.2254624E−07	−3.6469375E−06	1.1878968E−07	3.5193717E−07	1.7117284E−06	−3.5856704E−06
a_5	2.4871325E−10	3.9037251E−09	−7.2697865E−11	−2.0540668E−10	−1.1028285E−09	2.3057188E−09
a_6	−1.1493044E−13	−1.7306822E−12				

$\overline{\rho D}, \Phi_F = a_0 + a_1 T_S + a_2 T_S^2 + a_3 T_S^3 + a_4 T_S^4 + a_5 T_S^5 + a_6 T_S^6$ (298 K $\leqslant T_S$ (K) $\leqslant T_{WB}$).

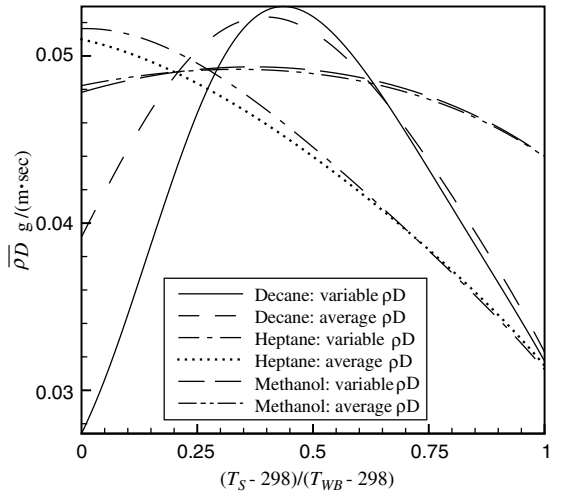

Fig. 6. Comparison of $\overline{\rho D}$ based on the constant ρD assumption with the exact value for decane, heptane, and methanol. $T_\infty = 298$ K, $Y_{O\infty} = 0.231$, with wet-bulb temperatures 429.73 K, 359.36 K, and 327.44 K for decane, heptane, and methanol.

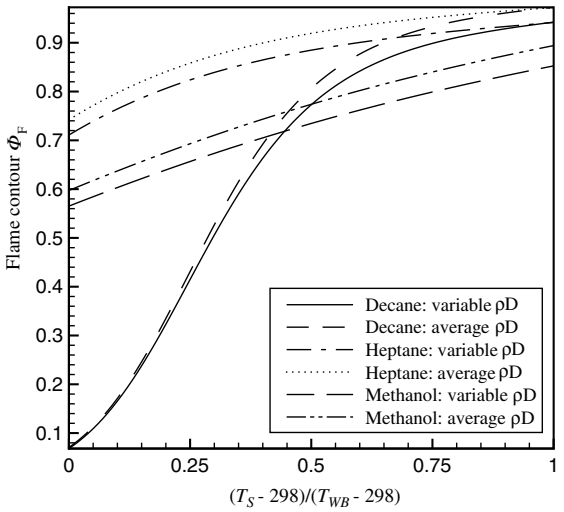

Fig. 7. Flame surface contour value computed with Eqs. (44) and (46) is shown versus surface temperature for decane, heptane, and methanol. $T_\infty = 298$ K, $Y_{O\infty} = 0.231$, with wet-bulb temperatures 429.73 K, 359.36 K, and 327.44 K for decane, heptane, and methanol.

$Y_{O\infty} = 0.75$. The overestimation of stand-off distances will also be present in multiple droplet arrays at wet-bulb temperatures. For all but the sparsest arrays, flames will be located at large distances from the array center so that a spherically symmetric solution is valid [11]. Although the error is less significant at lower liquid surface temperatures, a large fraction of the droplet lifetime is spent with the liquid surface near wet-bulb temperatures. Using a conduction-limit model [12], and with an ambience of air at 298 K, isolated decane and heptane droplets initially at 298K will have attained normalized surface temperatures of $(T_S - 298)/(T_{WB} - 298) = 0.5$ in approximately 0.5% of their total lifetime. Normalized surface temperatures of $(T_S - 298)/(T_{WB} - 298) = 0.75$ are attained in 3.3% and 2.1% of the total lifetimes for decane and heptane, respectively. Liquid-surface heating is even faster when $Y_{O\infty} > 0.231$. Therefore, "observed" flame locations would likely fall in the regime where liquid surface temperatures are near wet-bulb values and the over-prediction of flame location is substantial. Labowsky [3] indicates that an unsteady far-field may be responsible for the over prediction. Raghunandan and Mukunda [17] found that the use of variable properties for single droplets with unitary Lewis number reduced flame stand-off distances by almost a factor of two. The current finding agrees with [17], and shows that the assumption $\rho D =$ constant plays a large role in the over estimation of flame stand-off distances.

Still, even with variable properties, some over-prediction of stand-off distance is apparent. No experimental evidence about flame-stand-off exists for droplet arrays but the single-droplet results of Okajima and Kumagai [18] for heptane and Dakka and Shaw [19] for decane

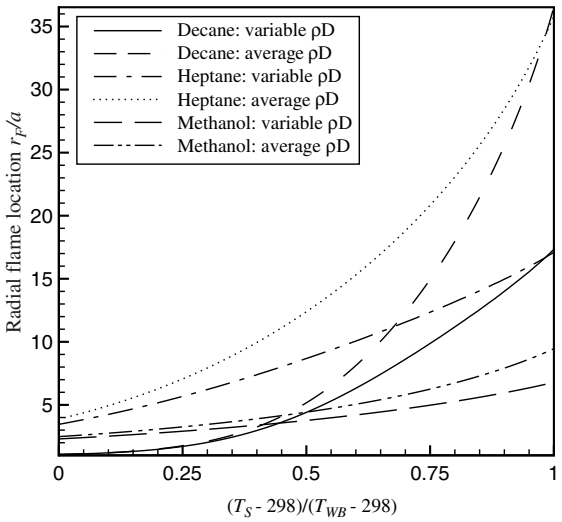

Fig. 8. Isolated droplet flame stand-off distances as computed with Eqs. (44) and (46) are shown versus surface temperature for decane, heptane, and methanol. $T_\infty = 298$ K, $Y_{O\infty} = 0.231$, with wet-bulb temperatures 429.73 K, 359.36 K, and 327.44 K for decane, heptane, and methanol.

are available. Our results are still somewhat higher for the special case of a spherically symmetric burning droplet. Raghunandan and Mukunda [17] found that a non-unitary Lewis further reduced stand-off distances by ~15%. Law and Law [20,21] produced theories for spherically symmetric droplet burning with non-unitary Lewis number and variable properties and without transient heating. For heptane, the predicted stand-off distance compares favorably with the experimental result of Okajima and Kumagai [18]. The theory with non-unitary Lewis number and a common mass-diffusivity [20] agreed quite well with experiment, indicating that a detailed transport description might not be needed. Certainly, there is reason to explore extension of the liquid-burning theory of this paper to the case of non-unitary Lewis number.

4. Conclusions

A generalized approach to liquid-fuel combustion problems for multiple-droplet arrays is presented. The gas-phase property analysis is independent of geometrical effects making the current analysis applicable in a variety of liquid configurations not limited to droplet arrays or sprays. The modification of burning rates due to droplet array size or configuration is dictated by the solution to the potential function that governs mass flux in the gas-phase, and satisfies Laplace's equation. Theoretical foundations for the existence of the mass flux potential function have been provided. Gas-phase scalar variables, transport properties, specific heats, and flame locations for a specified fuel type and boundary conditions depend only on the potential function and liquid surface temperature. Therefore, the problem for the scalar properties becomes one-dimensional for any configuration while the three-dimensional analysis is limited to the solution of Laplace's equation. Flame stand-off distances are found to decrease by more than a factor of two when the quantity ρD is not assumed constant. The effect of boundary conditions on transport properties and flame location is demonstrated. Correlations for coupling an unsteady liquid-phase to a quasi-steady gas-phase are provided.

References

[1] M. Labowsky, The effects of nearest neighbor interactions on the evaporation rate of cloud particles, Chem. Eng. Sci. 31 (1976) 803–813.
[2] M. Labowsky, A formalism for calculating the evaporation rates of rapidly evaporating interacting particles, Combust. Sci. Technol. 18 (1978) 145–151.
[3] M. Labowsky, Calculation of the burning rates of interacting fuel droplets, Combust. Sci. Technol. 22 (1980) 217–226.
[4] E.M. Twardus, T.A. Brzustowski, The interaction between two burning fuel droplets, in: Fifth International Symposium on Combustion Processes, Krakow Poland, vol. 8, 1977.
[5] T. Brzustowski, E.M. Twardus, S. Wojcicki, A. Sobiesiak, Interaction of two burning fuel droplets of arbitrary size, AIAA J. 17 (1979) 1234–1242.
[6] A. Umemura, S. Ogawa, N. Oshima, Analysis of the interaction between two burning droplets, Combust. Flame 41 (1981) 45–55.
[7] A. Umemura, S. Ogawa, N. Oshima, Analysis of the interaction between two burning fuel droplets with different sizes, Combust. Flame 43 (1981) 111–119.
[8] K. Sivasankaran, K.N. Seetharamu, R. Natarajan, Numerical investigation of the interference effects between two burning fuel spheres, Int. J. Heat Mass Transfer 39 (18) (1996) 3949–3957.
[9] M. Marberry, A.K. Ray, K. Leung, Effect of multiple particle interactions on burning droplets, Combust. Flame 57 (1984) 237–245.
[10] T. Elperin, B. Krasovitov, Analysis of evaporation and combustion of random clusters of droplets by a modified method of expansion into irreducible multipoles, Atomizat. Sprays 4 (1994) 79–97.
[11] R.T. Imaoka, W.A. Sirignano, Vaporization and combustion in three-dimensional droplet arrays, Proc. Combust. Inst. 30 (2005) 1981–1989.
[12] R.T. Imaoka, W.A. Sirignano, Transient vaporization and burning in dense droplet arrays, Int. J. Heat Mass Transfer, in press, doi:10.1016/j.ijheatmasstransfer.2005.05.012.
[13] D.D. Joseph, T.Y. Liao, Potential flows of viscous and viscoelastic fluids, J. Fluid Mech. 265 (1994) 1–23.
[14] D.D. Joseph, Viscous potential flow, J. Fluid Mech. 479 (2003) 191–197.

[15] C.K. Law, Unsteady droplet combustion with droplet heating, Combust. Flame 26 (1976) 17–22.
[16] C.K. Law, W.A. Sirignano, Unsteady droplet combustion with droplet heating-II: conduction-limit, Combust. Flame 28 (1977) 175–186.
[17] B.N. Raghunandan, H.S. Mukunda, The problem of liquid droplet combustion—a reexamination, Combust. Flame 30 (1977) 71–84.
[18] S. Okajima, S. Kumagai, Further investigations on combustion of free droplets in a freely falling chamber including moving droplets, in: Fifteenth Symposium (International) on Combustion, vol. 15, The Combustion Institute, 1975, pp. 401–407.
[19] S.M. Dakka, B.D. Shaw, Combustion of propanol droplets in reduced gravity, in: Proceedings of the Western States Section, The Combustion Institute, 2004.
[20] C.K. Law, H.K. Law, Quasi-steady diffusion flame theory with variable specific heats and transport coefficients, Combust. Sci. Technol. 12 (1976) 207–216.
[21] C.K. Law, H.K. Law, Theory of quasi-steady diffusional combustion with variable properties including distinct binary diffusion coefficients, Combust. Flame 29 (1977) 269–275.